

Article

Study on Osseointegration Capability of β -Type Ti–Nb–Zr–Ta–Si Alloy for Orthopedic Implants

Yu Sun ¹, Qingping Liu ², Zhenglei Yu ², Luquan Ren ², Xin Zhao ^{1,*} and Jincheng Wang ^{1,*}

¹ Orthopaedic Medical Center, The Second Hospital of Jilin University, Changchun 130041, China; yusun@jlu.edu.cn

² Key of Bionic Engineering, Ministry of Education, Jilin University, Changchun 130022, China; liuqp@jlu.edu.cn (Q.L.); zlyu@jlu.edu.cn (Z.Y.); lqren@jlu.edu.cn (L.R.)

* Correspondence: zhaoxin429@hotmail.com (X.Z.); wangjincheng2008@163.com (J.W.)

Abstract: Osseointegration is the basic condition for orthopedic implants to maintain long-term stability. In order to achieve osseointegration, a low elastic modulus is the most important performance indicator. It is difficult for traditional titanium alloys to meet this requirement. A novel β -titanium alloy (Ti–35Nb–7Zr–5Ta)₉₈Si₂ was designed, which had excellent strength (a yield strength of 1296 MPa and a breaking strength 3263 MPa), an extremely low elastic modulus (37 GPa), and did not contain toxic elements. In previous in vitro studies, we confirmed the good biocompatibility of this alloy and similar bioactivity to Ti–6Al–4V, but no in vivo study was performed. In this study, Ti–6Al–4V and (Ti–35Nb–7Zr–5Ta)₉₈Si₂ were implanted into rabbit femurs. Imaging evaluation and histological morphology were performed, and the bonding strength and bone contact ratio of the two alloys were measured and compared. The results showed that both alloys remained in their original positions 3 months after implantation, and neither imaging nor histological observations found inflammatory reactions in the surrounding bone. The bone–implant contact ratio and bonding strength of (Ti–35Nb–7Zr–5Ta)₉₈Si₂ were significantly higher than those of Ti–6Al–4V. The results confirmed that (Ti–35Nb–7Zr–5Ta)₉₈Si₂ has a better osseointegration ability than Ti–6Al–4V and is a promising material for orthopedic implants.

Keywords: β titanium alloy; low elastic modulus; osseointegration; bone–implant contact



Citation: Sun, Y.; Liu, Q.; Yu, Z.; Ren, L.; Zhao, X.; Wang, J. Study on Osseointegration Capability of β -Type Ti–Nb–Zr–Ta–Si Alloy for Orthopedic Implants. *Materials* **2024**, *17*, 472. <https://doi.org/10.3390/ma17020472>

Academic Editors: David Gillam, Javier Gil and Luciana Fávoro Francisconi-dos-Rios

Received: 1 December 2023

Revised: 9 January 2024

Accepted: 17 January 2024

Published: 19 January 2024



Copyright: © 2024 by the authors. Licensee MDPI, Basel, Switzerland. This article is an open access article distributed under the terms and conditions of the Creative Commons Attribution (CC BY) license (<https://creativecommons.org/licenses/by/4.0/>).

1. Introduction

Bone replacement implants are products that replace part of bone tissue to fulfill its function. Therefore, bone implants must be mechanically stable (e.g., high strength, fatigue resistant, abrasion and corrosion resistant, etc.) and biologically stable (low cytotoxicity and good osseointegration). The definition of osseointegration was proposed by Brånemark [1]. It refers to “the process resulting in direct structural and functional connection between ordered, living bone and the surface of a (load-bearing) implant” [2]. The basis of osseointegration is that the elastic modulus of the material is close to that of the bone tissue, so as to minimize the reduction in the strength of the surrounding bone tissue caused by the stress-shielding effect.

In order to find the ideal bone replacement materials, researchers have developed a series of titanium and titanium alloy materials. Among them, the most successful commercialization is the Ti–6Al–4V alloy [3–10]. Due to its good biocompatibility and relatively low elastic modulus (110 GPa), Ti–6Al–4V has become a versatile artificial joint prosthesis material. The application of Ti–6Al–4V has greatly contributed to the development of medical metal materials, but two toxic elements, vanadium (V) and aluminum (Al) are used in this type of alloy. In the 1980s, it was reported that the bone tissue around the Ti–6Al–4V artificial hip prosthesis appeared to be melanistic and infected. Studies have confirmed that V is highly toxic and can induce cancer by accumulating in various organs as a permanent

implant [11,12]. After Al is absorbed, it can cause bone malacia, nervous system disorders, anemia, etc., and it may also be related to Alzheimer's disease [7,9,13,14]. Moreover, the higher elastic modulus of Ti-6Al-4V compared to that of bone tissue (30 GPa) still cannot completely eliminate the stress-shielding effect.

Third-generation titanium alloys (β type alloys) contain biocompatible elements, such as Ti, Zr, Nb, Ta, Si, and Sn, which can also stabilize the β structure in titanium [14–19]. Overall, β -titanium alloys exhibit an elastic modulus closer to that of human bone, as well as improved biocompatibility [20,21]. In addition, the enhanced strength, plasticity, and good wear resistance properties make these alloys more suitable for use in biomedical implantation [22–26].

Numerous studies show that the grain size of the material has an effect on its mechanical properties. Compared with the coarse-grained material of the same composition, the fine-grained material has improved strength, plasticity, hardness, toughness, and wear resistance. La et al. [27] studied the tribological properties of Ti with different grain sizes in various environments, and the result was that ultrafine-grained Ti had better tribological properties than coarse-grained Ti. As far as biomedical alloys are concerned, in addition to better mechanical properties, fine-grained materials have better biological activity. Khang [28] and Webste [29] compared the effect of grain size on cell biocompatibility and adhesion behavior in pure titanium or titanium alloys with the same composition. The results show that the ultrafine-grained alloys and nano-alloys have higher surface energies and exhibit stronger osteoblast adhesion than the fine-grained alloys.

According to the design theory of d-electron alloy design, Li et al. have produced a new type of ultra-fine-grained titanium alloy fabricated via the spark plasma sintering (SPS) method [30]. The nominal composition is (Ti-35Nb-7Zr-5Ta)₉₈Si₂. The Ti-35Nb-7Zr-5Ta alloy system, which has been proven to have a low elastic modulus and good biocompatibility [24,31], was selected, and a Si element with improved biocompatibility was added to promote grain refinement and amorphous formation [22,31–34]. The alloy system has a low elastic modulus (as low as 37 GPa). The two-phase ultrafine microstructure includes body-centered cubic β -Ti matrix and (Ti, Zr)₂Si reinforcement phase. Its special deformation mechanism endows it with higher strength (a yield strength of 1296 MPa and a breaking strength of 3263 MPa). Its excellent mechanical compatibility far exceeds that of the widely used Ti-6Al-4V alloy, and it has enormous application potential.

In previous studies, we verified the improved biocompatibility of this novel (Ti-35Nb-7Zr-5Ta)₉₈Si₂ alloy through in vitro studies and found that its biological activity is comparable to that of commercialized Ti-6Al-4V [35]. In this study, we further evaluated the osseointegration capacity of this alloy by implanting the material into the bones of rabbits.

2. Experimental

2.1. Preparation of TiNbZrTaSi Specimens

(Ti-35Nb-7Zr-5Ta)₉₈Si₂ alloy was prepared as previously described [30]. Briefly, high-purity powders of Ti, Nb, Zr, Ta, and Si were mixed in a mechanical mixer for 4 h at 100 rpm. Subsequently, the mixture was subjected to high-energy ball milling at a rotational speed of 4.1 s⁻¹ under the protection of purified argon gas. After grinding, the powder sample was loaded into a graphite mold and sintered on an SPS-825 system (Sumitomo Coal Mining Co., Ltd., Tokyo, Japan). The alloy was sintered at a vacuum of 1233 K at a pressure of 50 MPa for 5 min. The sintered bulks were cut into cylindrical specimens (Φ 2 mm \times 10 mm), as shown in Figure 1. The commercial titanium alloy Ti-6Al-4V (AK Medical Co., Ltd., Beijing, China) was used as the control group. All specimens were polished, ultrasonically, cleaned with distilled water, an acetone solution, and 70% ethanol for 20 min. Then, they were ultrasonicated with distilled water for 15 min, autoclaved at 121 °C for 40 min, and vacuum-dried. SEM images showed that the polished (Ti-35Nb-7Zr-5Ta)₉₈Si₂ and Ti-6Al-4V alloy samples had glossy surfaces and scratches in the same direction [35].

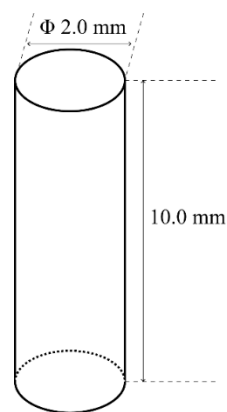


Figure 1. Geometry of the implants.

2.2. Surgical Procedures

The animal experiment was approved by the Ethical Committee for Animal Experiments of Jilin University of China. Six New Zealand white rabbits were used in the experiments, with no regard to gender. $(\text{Ti}-35\text{Nb}-7\text{Zr}-5\text{Ta})_{98}\text{Si}_2$ and Ti-6Al-4V were implanted into the left and right femurs of rabbits, respectively, and three specimens were implanted into each femur. The specific surgical methods were as follows: animals were placed in prone position, and 3% sodium pentobarbital was injected into the ear vein at a rate of 1 mL/kg for anesthesia. The left and right hind limbs were shaved to expose the skin at the femur, sterilized with iodine, and a sterile towel was laid out. The skin and subcutaneous tissue were incised, muscles were separated, and the periosteum was incised to expose the femoral shaft. On the lateral side of the femoral shaft, three holes with a diameter of 1.8 mm were drilled a low-speed drill in sequence, with a depth of about 10 mm and a hole spacing of 10 mm. During drilling, the local tissue was cooled with normal saline to prevent high temperature necrosis of the surrounding bone tissue. The specimens were inserted in the hole. After the surgery, the wound was subcutaneously closed with 4-0 nylon sutures. In the animal facility of the Laboratory Animal Center of Jilin University in China, the rabbits were housed in separate metal cages and moved freely in their cages. These animals were given specialized food and had access to water at will. Basic biological functioning, eating and excretion, behavioral signs associated with postoperative pain were carefully checked daily, and suture care for postoperative infection and surgical wounds, bleeding, and/or infection were monitored. After surgery and during the following three days, the animals received penicillin (8000 iu, qd, i.v.) and a 2% solution of tramadol hydrochloride (1.0 mg/kg, q12h, s.q.). The skin sutures were removed from the wound within ten days after the implantation surgery.

2.3. Imaging Observation

X-ray films were taken three months after the specimens were implanted into the animals' femurs, to evaluate the location of the implanted specimens in the bone and their surrounding tissue.

2.4. Osseointegration Strength

After the X-ray films were taken, the animals were sacrificed by overdose of 3% pentobarbital. The femurs were exposed, and a visual observation was conducted to determine the presence of redness, purulence, necrosis, and a gap between the implants and the surrounding tissue. The femurs were removed and the femur specimens of three animals were used for hard tissue sectioning and staining, while the other specimens were used for push-out experiments.

Both ends of the femurs were cut off with a diamond wheel (Figure 2a), and the femoral samples were put on a metal base with a V-groove for fixation. The implanted specimens were pushed axially with a 1.8 mm diameter thimble (Figure 2b). The mechanical push-out experiment was carried out on a universal mechanical machine. The loading speed was set to 1 mm/min, and the force-offset curve was recorded.

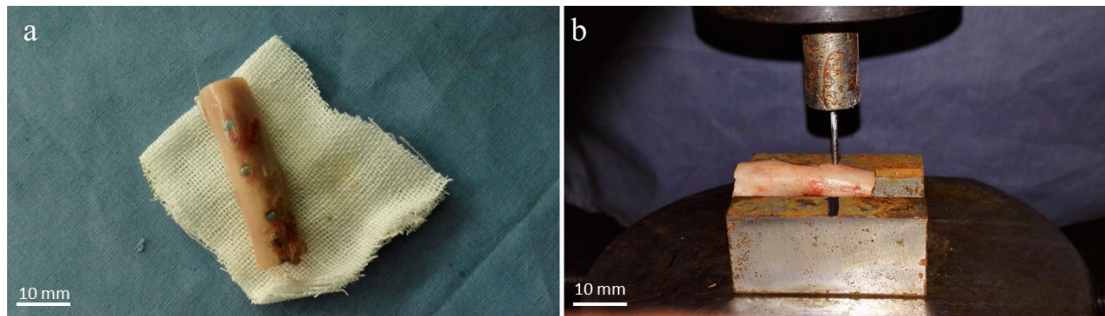


Figure 2. Push-out test operation. (a) The femur sample containing implants. (b) The implanted specimens were pushed axially with a 1.8 mm diameter thimble.

2.5. Histological Preparation

Specimens were processed using methacrylate embedding techniques [36].

The rabbit femurs with alloy specimens were fixed in 10% formalin for two weeks and then dehydrated with alcohols at different concentrations (70%, 80%, 96%, 99.8%, respectively) under constant agitation.

Plastic permeation was carried out under continuous agitation (Exakt 510) and under vacuum according to the following procedure: (1) Technovit 7200[®]/BPO:alcohol = 30:70. (2) Technovit 7200[®]/BPO:alcohol = 50:50. (3) Technovit 7200[®]/BPO:alcohol = 70:30. (4) Technovit 7200[®]/BPO. (5) Technovit 7200[®]/BPO. Each procedure was carried out for three days.

The specimens were light-cured with Technovit 7200 VLC solution (Morphisto, Offenbach am Main, Germany) in the EXAKT E520 light-curing embedding machine (EXAKT Advanced Technologies GmbH, Norderstedt, Germany) for 12 h, cut into sections with a thickness of about 200 μm with the EXAKT E300CP hard tissue microtome, and then polished with 800 mesh, 1200 mesh, and 4000 mesh sandpaper using the EXAKT E400CS tissue grinder to make sections with a thickness of about 70 μm for staining.

2.6. Histomorphology

The sections containing Ti-6Al-4V and $(\text{Ti}-35\text{Nb}-7\text{Zr}-5\text{Ta})_{98}\text{Si}_2$ were stained with HE, Masson, and toluidine blue, respectively. The bone-to-implant contact (BIC) rate was measured by an image information management software, Image-Pro Plus vision 6.0 (MediaCybernetic, Silver Springs, MD, USA).

2.7. Statistical Analysis

Results were presented as the mean \pm standard deviation. Differences between treatment groups were analyzed using a *t* test. Differences with $p < 0.05$ were considered statistically significant.

3. Results

3.1. Imaging Observation

All of the experimental animals were recovered from the implant surgery without any operative or postoperative complications. X-rays can show the location of the implant and the condition of the surrounding bone. It is shown in Figure 3 that all the Ti-6Al-4V and $(\text{Ti}-35\text{Nb}-7\text{Zr}-5\text{Ta})_{98}\text{Si}_2$ specimens were in their original positions without displacement. No obvious inflammatory reaction, osteoporosis, and lucid zone were observed in the

surrounding bone of the specimens. At the same time, a periosteal reaction could be observed around the specimens.



Figure 3. X-ray image of rabbit femurs. R: right side of the image.

3.2. Osseointegration Strength

The femurs were exposed three months after the operation (as shown in Figure 4a). There was no local reaction such as redness, purulence, and tissue necrosis around the specimens. All the specimens were well integrated with the bone tissue, and their surfaces were covered with periosteum. No obvious gaps were observed.

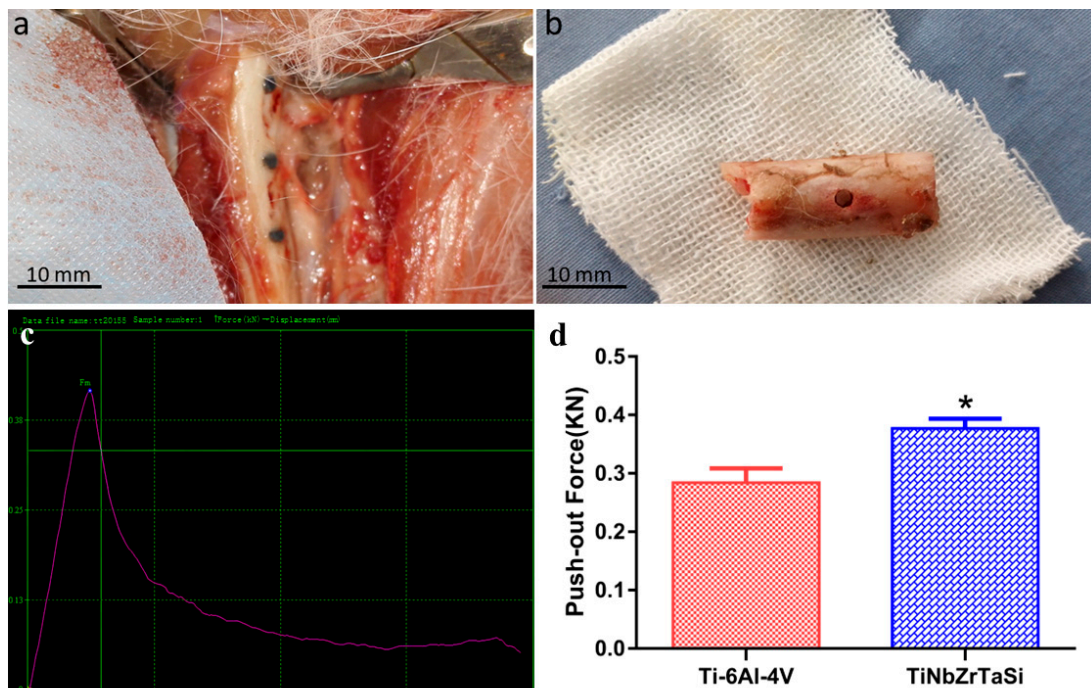


Figure 4. (a) The exposed femur containing implants three months after operation. (b) The femur sample after the implants were pushed out. (c) The force-offset curve. (d) The maximum pushing force analysis of $(\text{Ti}-35\text{Nb}-7\text{Zr}-5\text{Ta})_{98}\text{Si}_2$ and Ti-6Al-4V. (* $p < 0.05$).

In most studies, the maximum force during the push-out process is an indicator of the bond between the implant and the tissue. The force-offset curve showed in Figure 4c exhibited linearity before the maximum force point, and declined after the specimens were pushed out at the maximum force point. Figure 4d shows the statistical analysis results of the maximum pushing force of the two alloys. It can be observed that the maximum pushing force of $(\text{Ti-35Nb-7Zr-5Ta})_{98}\text{Si}_2$ ($377 \text{ N} \pm 17 \text{ N}$) was greater than that of Ti-6Al-4V ($284 \pm 25 \text{ N}$), and the difference between the two forces was significant ($p < 0.05$).

3.3. Histomorphology

HE staining, Masson staining, and toluidine blue staining were used to evaluate the tissue response around the implanted specimens and to measure the BIC rate. It can be observed from the HE-staining images that all specimens, whether $(\text{Ti-35Nb-7Zr-5Ta})_{98}\text{Si}_2$ or Ti-6Al-4V, were surrounded by extensive bone tissue. There was no obvious fibrosis and cysts. No material fragments and inflammatory cell infiltration were found at the implant–bone interface (Figure 5a,b).

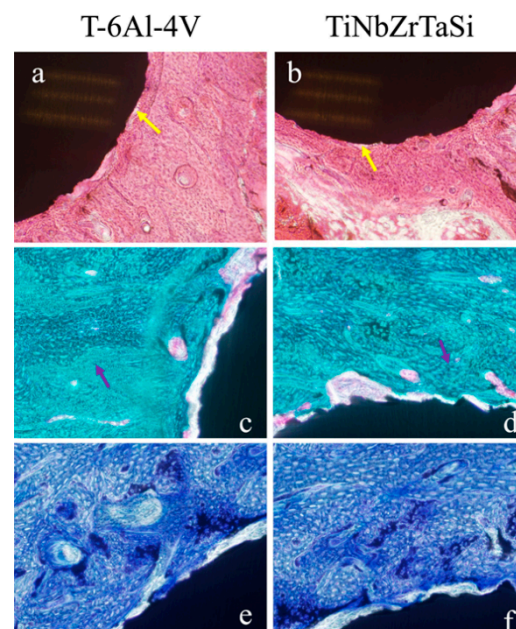


Figure 5. (a,b) HE staining sections of Ti-6Al-4V (a) and $(\text{Ti-35Nb-7Zr-5Ta})_{98}\text{Si}_2$ (b). Yellow arrows: gaps between implants and bone tissue. (c,d) Masson staining sections of Ti-6Al-4V (c) and $(\text{Ti-35Nb-7Zr-5Ta})_{98}\text{Si}_2$ (d). Purple arrows: new bone tissue. (e,f) Toluidine blue staining sections of Ti-6Al-4V (e) and $(\text{Ti-35Nb-7Zr-5Ta})_{98}\text{Si}_2$ (f).

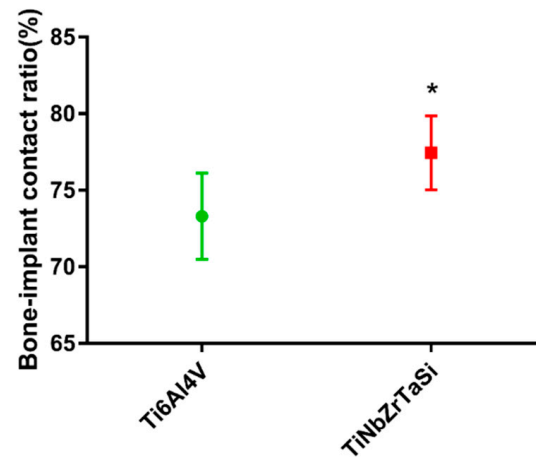
Masson staining can distinguish collagen and muscle fibers well and observe the maturity of bone tissue. It can be seen from the Masson staining photos that the implanted specimens were surrounded by a large amount of new bone tissue, and no fibrous tissue infiltration was observed in the implant–bone interface (Figure 5c,d).

Toluidine blue staining verified the results of Masson staining. In the toluidine blue-staining images, the new bone tissue dominated by osteoid appeared light blue, while the mineralized bone tissue and the specimens appeared dark blue and black, respectively (Figure 5e,f).

The BICs of the two samples were compared using the image analysis software Image-Pro Plus vision 6.0 (MediaCybernetic, Silver Springs, MD, USA). The 77.45% of $(\text{Ti-35Nb-7Zr-5Ta})_{98}\text{Si}_2$ was higher than the 73.31% of Ti-6Al-4V (Table 1), which was confirmed via statistical analysis to be significant (Figure 6) ($* p < 0.05$).

Table 1. The BIC ratio of Ti-6Al-4V and (Ti-35Nb-7Zr-5Ta)₉₈Si₂.

Implant	BIC (%)
Ti-6Al-4V	73.31 ± 1.07
(Ti-35Nb-7Zr-5Ta) ₉₈ Si ₂	77.45 ± 0.91 *

* $p < 0.05$.**Figure 6.** The BIC ratio of Ti-6Al-4V and (Ti-35Nb-7Zr-5Ta)₉₈Si₂ (* $p < 0.05$).

4. Discussion

In the process of manufacturing long-term functional implants, biocompatibility and long-term stability are the primary considerations, and the latter needs to be achieved through good osseointegration. In a previous study, we verified the good biocompatibility of the newly designed titanium alloy (Ti-35Nb-7Zr-5Ta)₉₈Si₂ through in vitro tests [35]. This study further evaluated the osseointegration properties of this alloy.

Osseointegration refers to the persistent bony contact between viable bone tissue and an implant. Branemark reported that the implanted pure titanium metal was unusually strongly bound to rabbit bone when studying the microcirculation in the bone marrow cavity and gave this definition for the first time to distinguish it from fibrous integration in histological characteristics [1]. The study of osseointegration involves a variety of methods, each with its own merits [37], and the comprehensive application of different methods can provide a more complete and detailed understanding of the tissue response and structural changes of the material–bone interface. Among them, X-ray, optical microscopy, histological analysis, biomechanical testing, etc. are more commonly used. In this study, X-ray, biomechanical, and histological analyses were selected to study the osseointegration of the interface between the materials and the bone tissue.

As a non-invasive test, X-rays can be used to observe the bone-material interface without causing damage to the animals. It can distinguish between bone, fibrous tissue, and inflammation in surrounding tissues by grayscale values. In this study, no gap was observed between the implant and the bone tissue. The bone tissue was directly bound to the materials, with no light transmission area being seen. And the surrounding tissue showed no signs of decreased bone density, demonstrating that the implant formed good osseointegration with the bone tissue and did not cause inflammatory changes or fibrous osteogenesis (Figure 3).

Theoretically, we can consider biomechanics to be the gold standard for measuring the degree of osseointegration. The better the degree of osseointegration, the stronger the bond between the material and the bone. The pull-out test is generally used for cylindrical implants inserted in the proximal and distal portion of long bones [38]. In this study, the push-out test was selected as a means to detect the bonding strength of (Ti-35Nb-7Zr-5Ta)₉₈Si₂ alloy and the bone interface, and the maximum push-out force was used as the criterion for evaluating the bonding strength (Figure 4). The maximum

push-out forces of (Ti–35Nb–7Zr–5Ta)₉₈Si₂ alloy and Ti-6Al-4V alloy reached 377 N and 284 N, respectively, indicating that the (Ti–35Nb–7Zr–5Ta)₉₈Si₂ alloy, whose elastic modulus is closer to that of human bone tissue, can effectively avoid the stress-shielding effect, promote the growth of surrounding bone tissue, and ensure the strength of the bone. In contrast, the biocompatibility and biological activity of the (Ti–35Nb–7Zr–5Ta)₉₈Si₂ alloy and the Ti-6Al-4V alloy were compared in our previous study, and the results confirmed that there was no significant difference between the two alloys [30]. The difference in the bonding strength of the two alloys should be attributed to differences in elastic modulus. Because the elastic modulus (37 GPa) of the TiNbZrTaSi alloy is closer to that of human bone tissue (30 GPa), its stress conduction is more even; thus, the surrounding bone tissue grows and rebuilds under stress, showing higher bonding strength [39].

Hard tissue sections can be used to make sections of bone tissue containing metal specimens without prior decalcification. The implant remains in situ, and the section can reflect the growth of the peri-implant bone tissue without destroying the original tissue structure of the implant–bone interface. We assessed the tissue response of the implant–bone interface through histomorphological observation and explored the reasons for the difference in the osseointegration strength of the two alloys. Hard tissue sections were stained with HE staining, Masson trichrome staining, and toluidine blue staining to observe the growth of inflammatory cells, osteoblasts, osteoclasts, fibrous tissue, and new bone. The BIC rate can be measured on histological sections, allowing for an intuitive evaluation of the ability of the material to directly bind to bone tissue. It can be observed from the HE-staining images that, although there was a partial gap at the implant–bone interface, no obvious inflammatory cell infiltration was observed (Figure 5a,b). This result was consistent with that from the previous study, in which we confirmed that none of the alloys caused the secretion of the inflammatory factor interleukin-6 (IL-6) [35]. Masson staining was mainly used to distinguish bone tissue and muscle fiber tissue and to evaluate the maturity of bone tissue. The results showed (Figure 5c,d) that after three months of implantation, the implants were surrounded by a large amount of new bone tissue, and no muscle fiber invasion was found in the implant–bone interface, indicating that the connection between the two was mainly bony rather than fibrous. Toluidine blue staining-images (Figure 5e,f) also showed massive new bone formation around the implants.

We measured the BIC rate on histological sections to verify the osseointegration effect of the two alloys. It can be observed (Figure 6) that the BIC rate of (Ti–35Nb–7Zr–5Ta)₉₈Si₂ (77.45%) was greater than that of Ti-6Al-4V (73.31%), and the difference was significant. According to the definition of osseointegration, more osseous connections between the implant and the surrounding bone and fewer fibrous connections lead to higher strength of the interface. This results in a more balanced biomechanical environment surrounding the implant and a better long-term stability of the implant. The higher BIC of (Ti–35Nb–7Zr–5Ta)₉₈Si₂ was consistent with the result of higher maximum push-out force. In the present study, the (Ti–35Nb–7Zr–5Ta)₉₈Si₂ alloy exhibited a larger BIC than the Ti-6Al-4V alloy, which in turn resulted in a higher osseointegration strength. This result was consistent with those of other related studies. Lin et al. [40] reported more new bone formation on the surface of low-elastic titanium alloys than high-elastic titanium alloys. Simon et al. [41] confirmed that low-elastic titanium alloys can promote good stress transfer, enhance the osseointegration of the implant, reduce bone resorption, and avoid the occurrence of prosthesis loosening. Stoppie et al. [42] used finite element analysis to confirm that the osseointegration rate and new bone thickness of the low-elastic implant were significantly higher than those of the high-elastic implant.

Bone remodeling is a long-term process, i.e., the occurrence of bone resorption and new bone formation is dynamic. The remodeling process can be clearly observed in the peri-implant area 6–12 weeks after implant installation. Most of the gaps are filled with mineralized bone, a mature bone tissue that is in close contact with the implant surface, resulting in successful osseointegration. The skeletal response in humans and animals

resembles load-induced bone remodeling that follows Wolf's Law, where bone tissue adapts to the load (or lack thereof) it is subjected to [43].

Obviously, the stresses and strains in the bone around the interface will counteract the load on the implant [2]. High interfacial stresses favor the formation of fibrous tissue and are associated with peri-implant bone damage. In addition, high interfacial stress can lead to increased micromotion at the implant–bone interface [44], resulting in nonmineralized fibrous tissue encapsulation [45], thus influencing osseointegration and bone remodeling [46,47]. Plenty of experimental studies have confirmed that a mismatch between the elastic modulus of the implant material and the bone tissue will cause the stress to be concentrated within the material itself as it passes through the implant. This stress cannot be well dispersed and transmitted to the bone tissue. This phenomenon is known as stress shielding [48–50]. Hedia [51] reported that a reduction in the modulus of elasticity can reduce stress concentrations. Therefore, it is reasonable to believe that the better osseointegration performance of the TiNbZrTaSi alloy in this study should be due to its relatively low elastic modulus.

Although there are important discoveries revealed by this study, there are also limitations. First, in this study, although we implanted three (Ti–35Nb–7Zr–5Ta)₉₈Si₂ alloys and three Ti–6Al–4V alloys in the two femurs of each rabbit, respectively, only nine samples were used for histological analysis and push-out test for each alloy. The sample size was relatively small compared to that of other studies; thus, false-positive results may appear. Secondly, although the surface treatment and morphology of the two metals were briefly described in this study, the surface roughness data could not be provided. This is a flaw in our study design. In summary, further improved research is necessary. First, the sample size needs to be enlarged. Second, control groups with different surface roughness need to be set up to exclude the effect of surface roughness on osseointegration results as much as possible.

Notwithstanding its limitation, this study does suggest that this new alloy with good biocompatibility [35] and a very low elastic modulus (~37 GPa vs. ~30 GPa of bone vs. ~110 GPa of Ti–6Al–4V) [14,30] has improved osseointegration ability and is a promising orthopedic implant material.

5. Conclusions

This new β -type titanium alloy with both high strength and a low elastic modulus has good biocompatibility. After the specimens were implanted in vivo, no inflammatory response of the surrounding tissue was triggered. When compared with Ti–6Al–4V, (Ti–35Nb–7Zr–5Ta)₉₈Si₂ exhibited higher osseointegration strength and BIC. Since we previously demonstrated that the bioactivities of the two alloys are similar, the improved osseointegration behavior of (Ti–35Nb–7Zr–5Ta)₉₈Si₂ should be attributed to its low elastic modulus. This alloy may be a superior implant material for biomedical application.

Author Contributions: Investigation, Q.L.; Resources, L.R.; Data curation, Z.Y. and X.Z.; Writing—original draft, Y.S.; Writing—review & editing, J.W. All authors have read and agreed to the published version of the manuscript.

Funding: This work was supported by the Jilin Provincial Natural Science Foundation (Grant number: YDZJ202201ZYTS046).

Institutional Review Board Statement: The animal study protocol was approved by the Ethics Committee for Animal Experiments of Jilin University of China (SY202202189, 1 May 2022).

Informed Consent Statement: Not applicable.

Data Availability Statement: Data are contained within the article.

Conflicts of Interest: The authors declare no conflicts of interest.

References

1. Branemark, P.-I. Osseointegration and its experimental background. *J. Prosthet. Dent.* **1983**, *50*, 399–410. [[CrossRef](#)] [[PubMed](#)]
2. Listgarten, M.A.; Lang, N.P.; Schroeder, H.E.; Schroeder, A. Periodontal tissues and their counterparts around endosseous implants. *Clin. Oral Implant. Res.* **1991**, *2*, 19. [[CrossRef](#)]
3. Anene, F.A.; Jaafar, C.N.A.; Zainol, I.; Hanim, M.A.A.; Suraya, M.T. Biomedical materials: A review of tita-nium based alloys. *Proc. Inst. Mech. Eng. Part C J. Mech. Eng. Sci.* **2020**, *235*, 3792–3805. [[CrossRef](#)]
4. Osak, P.; Maszybrocka, J.; Kubisztal, J.; Ratajczak, P.; Łosiewicz, B. Long-Term Assessment of the In Vitro Corrosion Resistance of Biomimetic ACP Coatings Electrodeposited from an Acetate Bath. *J. Funct. Biomater.* **2021**, *12*, 12. [[CrossRef](#)]
5. Łosiewicz, B.; Osak, P.; Maszybrocka, J.; Kubisztal, J.; Stach, S. Effect of Autoclaving Time on Corrosion Resistance of Sandblasted Ti G4 in Artificial Saliva. *Materials* **2020**, *13*, 4154. [[CrossRef](#)]
6. Froes, F.H.; Qian, M. *Titanium in Medical and Dental Applications*; Woodhead Publishing: Cambridge, UK, 2017. [[CrossRef](#)]
7. Chen, Q.Z.; Thouas, G.A. Metallic implant biomaterials. *Mater. Sci. Eng. R-Rep.* **2015**, *87*, 1–57. [[CrossRef](#)]
8. Abdel-Hady Gepreel, M.; Niinomi, M. Biocompatibility of Ti-alloys for long-term implantation. *J. Mech. Behav. Biomed. Mater.* **2013**, *20*, 407–415. [[CrossRef](#)]
9. Zhang, L.-C.; Chen, L.-Y. A Review on Biomedical Titanium Alloys: Recent Progress and Prospect. *Adv. Eng. Mater.* **2019**, *21*, 1801215. [[CrossRef](#)]
10. Wen, Y.; Xie, L.; Wang, Z.; Wang, L.; Lu, W.; Zhang, L.-C. Nanoindentation characterization on local plastic response of Ti-6Al-4V under high-load spherical indentation. *J. Mater. Res. Technol.* **2019**, *8*, 3434–3442. [[CrossRef](#)]
11. Cortizo, A.M.; Sa'lice, V.C.; Vescina, C.M.; Etcheverry, S.B. Proliferative and morphological changes induced by vanadium compounds on Swiss 3T3 fibroblasts. *Biomaterials* **1997**, *10*, 127–133. [[CrossRef](#)]
12. Silva, H.; Schneider, S.; Neto, C.M. Study of nontoxic aluminum and vanadium-free titanium alloys for biomedical applications. *Mater. Sci. Eng. C* **2004**, *24*, 679–682. [[CrossRef](#)]
13. Costa, B.C.; Tokuhara, C.K.; Rocha, L.A.; Oliveira, R.C.; Lisboa-Filho, P.N.; Pessoa, J.C. Vanadium ionic species from degradation of Ti-6Al-4V metallic implants: In vitro cytotoxicity and speciation evaluation. *Mater. Sci. Eng. C* **2018**, *96*, 730–739. [[CrossRef](#)] [[PubMed](#)]
14. Chen, L.-Y.; Cui, Y.-W.; Zhang, L.-C. Recent Development in Beta Titanium Alloys for Biomedical Applications. *Metals* **2020**, *10*, 1139. [[CrossRef](#)]
15. Anioek, K.; Losiewicz, B.; Kubisztal, J.; Osak, P.; Kaptacz, S. Mechanical Properties, Corrosion Resistance and Bio-activity of Oxide Layers Formed by Isothermal Oxidation of Ti-6Al-7Nb Alloy. *Coatings* **2021**, *11*, 505. [[CrossRef](#)]
16. Łosiewicz, B.; Stróż, A.; Osak, P.; Maszybrocka, J.; Gerle, A.; Dudek, K.; Balin, K.; Łukowiec, D.; Gawlikowski, M.; Bogunia, S. Production, Characterization and Application of Oxide Nanotubes on Ti-6Al-7Nb Alloy as a Potential Drug Carrier. *Materials* **2021**, *14*, 6142. [[CrossRef](#)]
17. Stróż, A.; Goryczka, T.; Łosiewicz, B. Electrochemical Formation of Self-Organized Nanotubular Oxide Layers on Niobium (Review). *Curr. Nanosci.* **2018**, *15*, 42–48. [[CrossRef](#)]
18. Szklarska, M.; Dercz, G.; Rak, J.; Simka, W.; Łosiewicz, B. The Influence of Passivation Type on Corrosion Resistance of Ti15Mo Alloy in Simulated Body Fluids. *Arch. Met. Mater.* **2015**, *60*, 2687–2694. [[CrossRef](#)]
19. Szklarska, M.; Dercz, G.; Simka, W.; Łosiewicz, B. Ac impedance study on the interfacial properties of passivated Ti13Zr13Nb alloy in physiological saline solution. *Surf. Interface Anal.* **2014**, *46*, 698–701. [[CrossRef](#)]
20. Zhang, L.C.; Klemm, D.; Eckert, J.; Hao, Y.L.; Sercombe, T.B. Manufacture by selective laser melting and mechanical behavior of a biomedical Ti-24Nb-4Zr-8Sn alloy. *Scr. Mater.* **2011**, *65*, 21–24. [[CrossRef](#)]
21. Zhang, L.C.; Chen, L.Y.; Wang, L.Q. Surface Modification of Titanium and Titanium Alloys: Technologies, Developments, and Future Interests. *Adv. Eng. Mater.* **2020**, *22*, 1901258. [[CrossRef](#)]
22. Abdi, S.; Khoshkhou, M.S.; Shuleshova, O.; Bönisch, M.; Calin, M.; Schultz, L.; Eckert, J.; Baró, M.D.; Sort, J.; Gebert, A. Effect of Nb addition on microstructure evolution and nanomechanical properties of a glass-forming Ti-Zr-Si alloy. *Intermetallics* **2013**, *46*, 156–163. [[CrossRef](#)]
23. Li, Y.; Yang, C.; Zhao, H.; Qu, S.; Li, X.; Li, Y. New Developments of Ti-Based Alloys for Biomedical Applications. *Materials* **2014**, *7*, 1709–1800. [[CrossRef](#)] [[PubMed](#)]
24. Brailovski, V.; Prokoshkin, S.; Gauthier, M.; Inaekyan, K.; Dubinskiy, S.; Petrzhik, M.; Filonov, M. Bulk and porous metastable beta Ti-Nb-Zr(Ta) alloys for biomedical applications. *Mater. Sci. Eng. C* **2011**, *31*, 643–657. [[CrossRef](#)]
25. Geetha, M.; Singh, A.K.; Asokamani, R.; Gogia, A.K. Ti based biomaterials, the ultimate choice for orthopaedic implants—A review. *Prog. Mater. Sci.* **2009**, *54*, 397–425. [[CrossRef](#)]
26. Matsumoto, H.; Watanabe, S.; Hanada, S. Beta TiNbSn alloys with low young's modulus and high strength. *Mater. Trans.* **2005**, *46*, 1070–1078. [[CrossRef](#)]
27. La, P.Q.; Ma, J.Q.; Zhu, Y.T.; Yang, J.; Lu, W.M.; Xue, Q.J.; Valiev, R.Z. Dry-sliding tribological properties of ultrafine-grained Ti prepared by severe plastic deformation. *Acta Mater.* **2005**, *53*, 5167–5173. [[CrossRef](#)]
28. Khang, D.; Lu, J.; Yao, C.; Haberstroh, K.M.; Webster, T.J. The role of nanometer and sub-micron surface features on vascular and bone cell adhesion on titanium. *Biomaterials* **2008**, *29*, 970–983. [[CrossRef](#)]
29. Webster, T.J.; Ejiiofor, J.U. Increased osteoblast adhesion on nanophase metals: Ti, Ti6Al4V, and CoCrMo. *Biomaterials* **2004**, *25*, 4731–4739. [[CrossRef](#)]

30. Yang, C.; Wang, F.; Zhao, H.; Qu, S.; Li, X.; Zhang, W.; Li, Y. Biomedical TiNbZrTaSi alloys designed by d-electron alloy design theory. *Mater. Des.* **2015**, *85*, 7–13. [[CrossRef](#)]
31. Calin, M.; Gebert, A.; Ghinea, A.C.; Gostin, P.F.; Abdi, S.; Mickel, C.; Eckert, J. Designing biocompatible Ti-based metallic glasses for implant applications. *Mater. Sci. Eng. C* **2013**, *33*, 875–883. [[CrossRef](#)]
32. Wilson, B.J. Designing media messages about health and nutrition: What strategies are most effective? *J. Nutr. Educ. Behav.* **2007**, *39* (Suppl. S2), S13–S19. [[CrossRef](#)] [[PubMed](#)]
33. Kuroda, D.; Niinomi, M.; Morinaga, M.; Kato, Y.; Yashiro, T. Design and mechanical properties of new β type titanium alloys for implant materials. *Mater. Sci. Eng. A* **1998**, *243*, 244–249. [[CrossRef](#)]
34. Cullity, B.D.; Smoluchowski, R. Elements of X-Ray Diffraction. *Phys. Today* **1957**, *10*, 50. [[CrossRef](#)]
35. Sun, Y.; Song, Y.; Zuo, J.L.; Wang, S.Q.; Gao, Z.L. Biocompatibility evaluation of novel β -type titanium alloy (Ti-35Nb-7Zr-5Ta)Si. *Rsc Adv.* **2015**, *5*, 101794–101801. [[CrossRef](#)]
36. von Wilmslow, C.; Moest, T.; Nkenke, E.; Stelzle, F.; Schlegel, K.A. Implants in bone: Part I. A current overview about tissue response, surface modifications and future perspectives. *Oral Maxillofac. Surg.* **2013**, *18*, 243–257. [[CrossRef](#)]
37. Robiony, M.; Polini, F.; Costa, F.; Politi, M. Osteogenesis distraction and platelet-rich plasma for bone restoration of the severely atrophic mandible: Preliminary results. *J. Oral Maxillofac. Surg.* **2002**, *60*, 630–635. [[CrossRef](#)] [[PubMed](#)]
38. Sanden, B.; Olerud, C.; Larsson, S. Hydroxyapatite coating enhances fixation of loaded pedicle screws: A mechanical in vivo study in sheep. *Eur. Spine J.* **2001**, *10*, 334–339. [[CrossRef](#)]
39. Sumner, D.R.; Turner, T.M.; Igloria, R.; Urban, R.M.; Galante, J.O. Functional adaptation and ingrowth of bone vary as a function of hip implant stiffness. *J. Biomech.* **1998**, *31*, 909–917. [[CrossRef](#)]
40. Lin, D.J.; Chuang, C.C.; Chern Lin, J.H.; Lee, J.W.; Ju, C.P.; Yin, H.S. Bone formation at the surface of low modulus Ti-7.5Mo implants in rabbit femur. *Biomaterials* **2007**, *28*, 2582–2589. [[CrossRef](#)]
41. Simon, U.; Augat, P.; Ignatius, A.; Claes, L. Influence of the stiffness of bone defect implants on the mechanical conditions at the interface—A finite element analysis with contact. *J. Biomech.* **2003**, *36*, 1079–1086. [[CrossRef](#)]
42. Stoppie, N.; Van Oosterwyck, H.; Jansen, J.; Wolke, J.; Wevers, M.; Naert, I. The influence of Young's modulus of loaded implants on bone remodeling: An experimental and numerical study in the goat knee. *J. Biomed. Mater. Res. Part A* **2009**, *90*, 792–803. [[CrossRef](#)] [[PubMed](#)]
43. Christen, P.; Ito, K.; Ellouz, R.; Boutroy, S.; Sornay-Rendu, E.; Chapurlat, R.D.; van Rietbergen, B. Bone remodelling in humans is load-driven but not lazy. *Nat. Commun.* **2014**, *5*, 4855. [[CrossRef](#)] [[PubMed](#)]
44. Brunski, J.B.; A Puleo, D.; Nanci, A. Biomaterials and biomechanics of oral and maxillofacial implants: Current status and future developments. *Int. J. Oral Maxillofac. Implant.* **2000**, *15*, 15–46.
45. Brunski, J.B. Biomechanical factors affecting the bone-dental implant interface. *Clin. Mater.* **1992**, *10*, 153–201. [[CrossRef](#)] [[PubMed](#)]
46. Szmukler-Moncler, S.; Salama, H.; Reingewirtz, Y.; Dubruille, J.H. Timing of loading and effect of micromotion on bone-dental implant interface: Review of experimental literature. *J. Biomed. Mater. Res.* **1998**, *43*, 192–203. [[CrossRef](#)]
47. Szmukler-Moncler, S.; Piattelli, A.; Favero, G.A.; Dubruille, J. Considerations preliminary to the application of early and immediate loading protocols in dental implantology. *Clin. Oral Implant. Res.* **2000**, *11*, 12–25. [[CrossRef](#)]
48. Huiskes, R.; Weinans, H.; VAN Rietbergen, B. The relationship between stress shielding and bone resorption around total hip stems and the effects of flexible materials. *Clin. Orthop. Relat. Res.* **1992**, *274*, 124–134. [[CrossRef](#)]
49. Gasser, B. *Design and Engineering Criteria for Titanium Devices*; Springer: Berlin/Heidelberg, Germany, 2001; pp. 673–701.
50. Shtansky, D.; Gloushankova, N.; Sheveiko, A.; Kharitonova, M.; Mozhess, T.; Levashov, E.; Rossi, F. Design, characterization and testing of Ti-based multicomponent coatings for load-bearing medical applications. *Biomaterials* **2005**, *26*, 2909–2924. [[CrossRef](#)]
51. Hedia, H.S. Stress and strain distribution behavior in the bone due to the effect of cancellous bone, dental implant material and the bone height. *Bio-Med. Mater. Eng.* **2002**, *12*, 111–119.

Disclaimer/Publisher's Note: The statements, opinions and data contained in all publications are solely those of the individual author(s) and contributor(s) and not of MDPI and/or the editor(s). MDPI and/or the editor(s) disclaim responsibility for any injury to people or property resulting from any ideas, methods, instructions or products referred to in the content.